

# Gradual Collective Upgrade of a Swarm of Autonomous Buoys for Dynamic Ocean Monitoring

Francesco Vallega

*SUTD-MIT International Design Center*  
Singapore University of Technology and Design  
Singapore  
francesco\_vallega@sutd.edu.sg

David Mateo

*Engineering Product Development*  
Singapore University of Technology and Design  
Singapore  
david\_mateo@sutd.edu.sg

Grgur Tokić

*Dept. of Mechanical Engineering*  
Massachusetts Institute of Technology  
Cambridge, USA  
gtokic@mit.edu

Roland Bouffanais

*Engineering Product Development*  
Singapore University of Technology and Design  
Singapore  
bouffanais@sutd.edu.sg

Dick K. P. Yue

*Dept. of Mechanical Engineering*  
Massachusetts Institute of Technology  
Cambridge, USA  
yue@mit.edu

**Abstract**—Swarms of autonomous surface vehicles equipped with environmental sensors and decentralized communications bring a new wave of attractive possibilities for the monitoring of dynamic features in oceans and other waterbodies. However, a key challenge in swarm robotics design is the efficient collective operation of heterogeneous systems. We present both theoretical analysis and field experiments on the responsiveness in dynamic area coverage of a collective of 22 autonomous buoys, where 4 units are upgraded to a new design that allows them to move 80% faster than the rest. This system is able to react on timescales of the minute to changes in areas on the order of a few thousand square meters. We have observed that this partial upgrade of the system significantly increases its average responsiveness, without necessarily improving the spatial uniformity of the deployment. These experiments show that the autonomous buoy designs and the cooperative control rule described in this work provide an efficient, flexible, and scalable solution for the pervasive and persistent monitoring of water environments.

**Index Terms**—Distributed Robotics, Collective behavior, Autonomous surface vehicle, Dynamic area coverage

## I. INTRODUCTION

Monitoring the ocean and coastal areas has traditionally been accomplished using either moored buoys or fixed networks of bulky, partially submerged platforms. The cost of developing, producing, deploying, and maintaining such systems has severely limited the range and precision of the sensed data obtained from monitoring large-scale waterbodies. To overcome these limitations, the community has started focusing on developing simpler, smaller, motorized, autonomous surface vehicles [1]–[5]. A large group of such vehicles operating as a collective can be deployed, retrieved, and re-deployed (partially or completely) at considerably lower cost and operational complexity than monolithic structures. Following the design paradigm of swarm robotics, these collectives perform complex tasks cooperatively in a scalable fashion, with a behavior that is both robust to failures and flexible so as to operate in dynamic environments [6], [7]. Moreover, a swarm

of mobile surface vehicles forms a dynamic sensor network suitable for high temporal sampling of waterbodies.

The pressing need for small, low-cost and rapidly deployable autonomous vehicles has been acknowledged in multiple recent reports [8]–[11]. However, using such large distributed systems for ocean monitoring presents as many possibilities as it does challenges. On the one hand, the system modularity and the individual cost of production primes them for iterative design and fast prototyping, in which field tests provide insights enabling a constant improvement toward future models. On the other hand, this iterative process is likely to produce an heterogeneous system, in which the agents have different motor, sensing, communication, or processing capabilities. This heterogeneous character must be properly handled at the system-level design in order to benefit from the range of agent capabilities.

We have previously reported on the design, construction, and testing of a homogeneous swarm of 50 (identical) autonomous buoys performing adaptive deployment for applications in environmental monitoring [12]. Here, we investigate and study the nontrivial process of partially upgrading this swarm robotics system by replacing a small fraction of the original swarming units (simply denoted v1) with upgraded robotic platforms (v2), based on a fully redesigned model featuring highly improved motor and processing capabilities among other things.

We have combined a set of 18 v1 buoys with 4 upgraded v2 buoys—hence constituting a heterogeneous swarm—and performed dynamic area coverage experiments in fully unstructured environments without the support of any external infrastructure when it comes to the system’s operations (see Fig. 1). We measured the collective responsiveness—a proxy to assess the flexible character of a swarm [13]—by changing the target area at different frequencies in order to investigate the minimum response time at which the heterogeneous swarm is able to adapt to changes in the monitored environment. For



Fig. 1. Swarm of buoys being deployed in the target area undergoing monitoring. Note that some units are still being deployed from the shore where the picture is taken.

this series of experiments on dynamic area coverage, the only practical differences between the two platforms are the speed of the units, their inertia, and their hull design. Specifically, design v2 is 80% times faster in open water and 2.3 times lighter than v1, thereby making it considerably more apt to quickly correct its position to adapt to changes in the target area undergoing monitoring. The field experiments performed reveal that the partial upgrade of the system is able to increase the average response of the system, but not necessarily the uniformity of the deployment.

## II. ROBOTIC PLATFORMS

In [12], we presented a study of dynamic ocean monitoring using a homogeneous swarm of 50 buoys. Such decentralized and cooperative systems primarily owe their outstanding effectiveness to the large number of agents put together: a greater number of agents allows for vaster waterbody coverage and/or refined multi-point sensing. As technology inexorably moves forward at an increasingly faster pace, there is a compelling opportunity to expand and upgrade at least some of the agents of the collective. These new units with improved capabilities have to be able to fit and operate within the technical framework of the original system.

The original buoy platform—design v1—is thoroughly described in [12], and we refer the reader to this report for full technical details. In this section, we focus on introducing an improved design (v2) and its main differences with respect to v1. This new design (see Fig 2), re-designed mainly to facilitate operation and maintenance, can be used to replace some units in the homogeneous swarm, or expand the original homogeneous system.

The platform has a modular design consisting of (i) a cylindrical hull, (ii) a top lid hosting the electronics on one side and antennas on the other, and (iii) a detachable bottom section that can be customized to host a number of environmental sensors, as shown in Fig. 2. The main hull for v2 is designed to provide the same omnidirectional vector propulsion apparatus as in v1, while encapsulating the three thrusters within the cylindrical shape and keeping them as close as possible to the center of gravity of the platform. This design choice

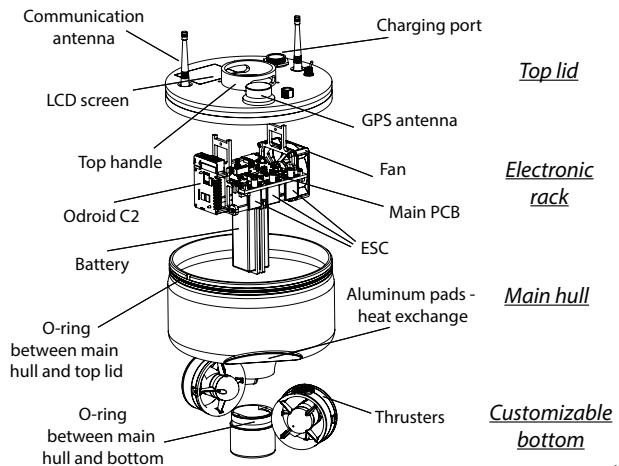


Fig. 2. Exploded view of the upgraded buoy design v2 displaying its modular design and main components.

stands in clear contrast with v1 that has protruding pairs of propellers, see Fig. 3. On the one hand, this new design minimizes the wobbling when the thrusters are active and provide a certain level of dynamic stability to the surface vehicle. On the other hand, the new hull has a larger packing density, which facilitates stackability and transportation of large numbers of platforms to remote field areas (see Fig. 1 in [12]). The mechanical design of v2 and the distribution of components inside the main hull has been designed and tested to not compromise the hydrostatics of v1, thereby retaining the critical self-righting feature of the v1 design.

The presence of three lateral aluminum pads allows for heat exchange between the water and the air inside the hull—a fan ensures adequate air circulation to homogenize the heat generated mainly by the 3 electronic speed controllers (ESC in Fig. 2) and the single-board computer Odroid C2. These aluminum pads can themselves host small sensors or light-emitting devices orientated 45 degrees below the water surface.

The top lid hosts the electronics and related hardware as a modular design itself. An electronic rack built around the main PCB and battery is screwed on the inside of this lid, thereby forming one single piece that can easily be replaced or disassembled for rapid inspection. Following the buoy v1 design, the outer part of the top lid hosts connectivity hardware such as communication and GPS antennas, and a charging port. The top lid of v2 includes an LCD screen reporting a range of data and indicators, which greatly facilitates the basic inspection and troubleshooting of the system’s digital status. Lastly, a mechanical handle has been incorporated into v2’s top lid design to aid both manual carrying and latching a stacked platform on top of it.

The bottom part is designed to securely host the battery, and can be modified to accommodate any sensor. The latter can be easily and conveniently interfaced with the electronic stack through a mini-PCI custom PCB that can be slotted inside the main PCB. This configuration was specifically designed to support further heterogeneity of the system at the sensing



Fig. 3. The two robotic platforms: the new buoy design v2 (left) side by side with one of the previous buoy model v1 (right).

level, with various units possibly carrying different sensors.

Particular attention has been placed on identifying a simple way of assembling parts and components. An example is the thruster attachment, in which a combination of a laser-cut gaskets and screws allows for servicing all three thrusters in less than 5 minutes—eight times faster than for the v1 design. In addition, the structure of the new electronics rack is composed of laser-cut acrylic sheets and designed using screwless joineries to facilitate manufacture, assembly and reduce potential leaks.

Once assembled, platform v2 measures  $260 \times 260 \times 245$  mm and weights 3.2 kg. For comparison, the previous design measures  $350 \times 350 \times 280$  mm and weights 7.4 kg. The reduction in dimensions is primarily achieved by moving from a spherical form to a cylindrical one, which allows for a compact embedding of the thrusters. The reduction in weight comes from using plastic material for the hull as opposed to aluminum alloy in v1. Besides weight reduction, the usage of 3D printed nylon plastic material inherently prevents corrosion and safely withstands seawater conditions, while reducing the amount of biofouling accumulating on the platform during operations as compared to metal. Due to the low number of v2 prototypes, the plastic hulls have been 3D-printed, making the cost comparable with the aluminum hull of v1. However, when mass producing the units using plastic injection inside a mold, the cost per unit is expected to be significantly lowered.

#### *Performance comparison: buoy v1 vs. v2*

Fig. 3 shows a visual comparison between buoy v1 and one of the prototypes of the improved design v2. By incorporating the thrusters into the main hull, buoy v2 is much more compact and increases the propellers' life—the propellers are protected as compared to v1 in which the protruding pods and open propellers can easily be damaged during transportation and/or operation.

A series of performance tests were carried out under different environmental conditions to offer a detailed comparison of the two platforms. The tests were run over a distance of

100 m in the direction of the prevailing the wind and against it. The platforms were initially positioned next to one another so as to obtain results under the practically identical conditions. The three BlueRobotics T100 thrusters allow the buoy v2 to move about 80% faster than v1 in nominal test operations, although the thrusters are capable of performing at much higher intensity.

This self-imposed limitation on the thrusters' intensity is purely related to the need to develop a more complex vectorial propulsion system than v1's. However, since the cooperative control strategy remains the same for v1 and v2 when performing the heterogeneous swarming tests, it was decided to not use the full power of the thrusters of v2. When testing the two platforms, side by side, in adverse environmental conditions—strong winds, waves and heavy rains, the performance of v2 was practically unaffected. On the contrary, buoy v1 drastically underperformed, with instances at which it was fully unable to reach its target goal.

It is worth noting that buoy v2 is granted a battery 1.5 bigger than the one in v1 to compensate the need for higher power by the thrusters, and the extra electronics energy consumption due to fan and LCD.

### III. DYNAMIC AREA COVERAGE

#### *A. Collective Operations*

Our multi-robot system can perform a range of collective behaviors achieved by means of a cooperative control strategy supported by distributed communications as described in full details in [12]. For instance, this distributed robotic system can perform a number of elementary swarming behaviors, including flocking, navigation, and area coverage. The effectiveness of the distributed communication setup has been verified and analyzed in [12].

This large-scale networked array of mobile sensing units is designed to monitor and characterize waterbodies, which may vary depending on the application. An example is the deployment of the swarm of buoys in a harbor to assist in marine operations by monitoring key environmental and flow parameters. More interestingly, the area to monitor might not be specified externally or in advance, but instead be defined dynamically by the collective of agents itself. By local processing of the sensed data, the agents may determine the shape in which to self-deploy in order to track a particular temperature profile, oil spill, or a range of biological markers.

#### *B. Cooperative Control for Dynamic Area Coverage*

As discussed in the previous section, the distributed robotic systems are designed to monitor features of interest in waterbodies (e.g. oil spills, algal blooms, etc.). To do so, we require the agents to spread as uniformly as possible across a given area that dynamically evolves over time.

It is paramount for this spreading to happen in a timely and responsive way, as the shape of the area of interest is in general time-changing with arbitrary dynamics. For this reason, we choose to define the behavior of the agents in a purely Markovian fashion with agent's dynamical rules

that determine the buoys' movements based solely on the instantaneous state, i.e. the cooperative control algorithm for agent  $i$  can be cast as

$$\frac{d\vec{r}_i}{dt} = \vec{F}(t, \vec{r}_i(t), \{\vec{r}_j(t)\}_{j \sim i}). \quad (1)$$

where  $\vec{r}_i$  is the position of a given agent  $i$ , and  $j \sim i$  is the set of agents in the neighborhood of  $i$ —its “neighbors” according to a specified interaction distance, be it metric, topological or else [14].

The area of interest is typically determined either by external sources (e.g. a human operator) or by the sensing capabilities of the agents (e.g. collective tracking of a temperature gradient, or chemical concentration, etc.). For the sake of generality, we assume that the area to monitor can be described mathematically by

$$A(\vec{r}) < 0, \quad (2)$$

where  $A$  is a signed distance function (or at least a function that increases monotonically outside the region). Given (2), the cooperative control rule is defined as

$$\frac{d\vec{r}_i}{dt} = v_{0i} \frac{\vec{T}}{\max(1, \|\vec{T}\|)}, \quad (3)$$

where  $v_{0i}$  is the maximum speed of an agent  $i$  and  $\vec{T}$  is the “area coverage target” defined by

$$\vec{T} = \frac{1}{1 + \exp(-\beta A(\vec{r}_i))} \frac{-\vec{\nabla} A}{\|\vec{\nabla} A\|} - \sum_{j \sim i} \frac{a_R^d}{r_{ij}^d} \frac{\vec{r}_{ij}}{r_{ij}}. \quad (4)$$

The first term in (4), proportional to  $-\vec{\nabla} A$ , attracts the agents towards the interior of the area and is scaled in such a way that its norm goes from being practically zero outside the area to cover ( $A > 0$ ) to being unity inside it ( $A < 0$ ). The parameter  $\beta$  controls how abruptly the transition between zero and one is, i.e. the steepness of the exponential decrease. The second term is an inter-agent repulsion term that causes the agents to spread inside the area. The type of repulsion is controlled by two parameters, namely the repulsion strength  $a_R$  and the power of repulsion  $d$ . If the power  $d$  is large ( $d \gtrsim 4$ ), the repulsion strength is approximately equal to the nearest-neighbor distance in equilibrium configurations.

Following numerical optimization run over simulations of the behavior (4), we set the free parameters to

$$d = 6, \quad a_R = 0.38\sqrt{S/N}, \quad \beta = 40/S, \quad (5)$$

where  $S$  is the total surface area to cover and  $N$  the number of agents.

### C. Target Surface to Monitor

As a testbed for dynamic area exploration, we consider the following surface

$$A_{\alpha, \hat{e}}(\vec{r}) = r^2 - R_{\alpha, \hat{e}}^2(\hat{r}), \quad (6)$$

where

$$R_{\alpha, \hat{e}}(\hat{r}) = \frac{R_0}{2} \frac{2 - \alpha + 3\alpha(\hat{r} \cdot \hat{e})^2}{\sqrt{1 + \alpha/2 + 11\alpha^2/32}}, \quad (7)$$

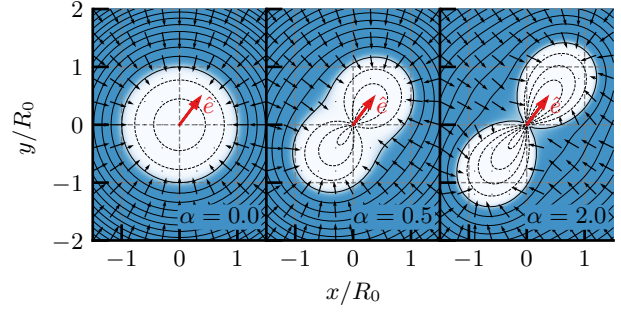


Fig. 4. Effect of the geofencing term for the area given by (6). The arrows show the vector field of the first term in (4), and the color gradient maps its norm. The contour lines mark isolines  $A_{\alpha, \hat{e}}$ .

By changing  $\alpha$ , the shape of this region goes from a disk of radius  $R_0$  ( $\alpha = 0$ ), to a two-lobbed area along the principal axis  $\hat{e}$  ( $\alpha = 1$ ), to a “dumbbell-shaped” region with a nodal point at the origin ( $\alpha = 2$ ). The normalization factor in (7) is introduced so that the total surface of the area is kept constant at  $S = \pi R_0^2$  for any  $\alpha \in [0, 2]$ . The gradient of this surface is

$$\nabla A_{\alpha, \hat{e}}(\vec{r}) = 2\vec{r} - 6\alpha R_0 \frac{R_{\alpha, \hat{e}}(\hat{r})}{r} (\hat{r} \cdot \hat{e}) \hat{e}_\perp, \quad (8)$$

where  $\hat{e}_\perp = \hat{e} - (\hat{r} \cdot \hat{e})\hat{r}$  is the orthogonal projection of the principal axis  $\hat{e}$  on the position  $\vec{r}$ . The attractive geofencing force field corresponding to this target surface is presented in Fig. 4. The contours depict the lines of constant  $A_{\alpha, \hat{e}}$  and the arrows show the vector field of the first term of (4) for three values of  $\alpha$ .

## IV. THEORETICAL ANALYSIS

We can study the performance of the cooperative rule (4) in *dynamic* area coverage by imposing a cyclic temporal evolution of the shape of the monitoring area at different frequencies.

To quantify the response of the system, we consider two metrics for the dynamic coverage performance that were previously used when testing with a homogeneous swarm [12]. The first one is the “tessellation performance”  $P_T$ , defined as the inverse of the relative size of the largest cell assigned to any agent after segmenting the target area with a Voronoi tessellation, or

$$P_T = \frac{A}{A_{LVC}N}, \quad (9)$$

where  $A$  is the total area of the target surface,  $A_{LVC}$  is the area of the largest Voronoi cell (dark cell in the inset of the top panel in Fig. 5), and  $N$  is the number of agents.

The second metric is the so-called “coverage performance”  $P_C$ , defined as the percentage of the target area covered by the agents (assuming each agent covers a disk of a certain radius  $R_s$  around its position), or

$$P_C = \frac{\bigcup_{i=1}^N c_i \cap A}{A}, \quad (10)$$



where  $c_i$  is a disk of radius  $R_s$  centered at the position of agent  $i$  (see inset at the bottom of Fig. 5).

The tessellation performance is meant to capture the expected accuracy of the least accurate mobile sensing unit, since it only involves the largest Voronoi cell. The coverage performance, on the other hand, is a measure of the average quality of the deployment, i.e. a good proxy for system-level performance. Both metrics take only positive values lower than unity, and where the unity corresponds to an ideal coverage.

### A. Ideal Homogeneous Swarm

We first consider a swarm of  $N = 20$  agents following the dynamics given by Eq. (4) with a certain speed  $v_0$  identical for all the agents. We then study the responsiveness—a proxy to assess the flexible character of a swarm [13]—of the system when covering the surface (2) changing at a frequency  $\omega$  such that  $\alpha(t) = 1 - \cos \omega t$ . The particular values of  $R_0$  and  $v_0$  are arbitrary, as the behavior of the system only depends on the normalized frequency  $\bar{\omega} = \omega R_0 / v_0$ .

The collective response of a system following (4) is shown in Fig. 5. The obtained response, measured either with the tessellation or coverage metrics, can be fit to the form

$$P(\bar{\omega}) = \frac{P_0 \bar{\omega}_c^\lambda + P_\infty \bar{\omega}^\lambda}{\bar{\omega}_c^\lambda + \bar{\omega}^\lambda}, \quad (11)$$

where  $P_0$  and  $P_\infty$  are the limit performances for  $\omega \rightarrow 0$  and  $\omega \rightarrow \infty$  respectively,  $\bar{\omega}_c$  is the “cutoff frequency” of the system, and the exponent  $\lambda$  measures how steep the transition from  $P_0$  to  $P_\infty$  is. The values for these parameters obtained by fitting (11) to the results in Fig. 5 are given in Table I.

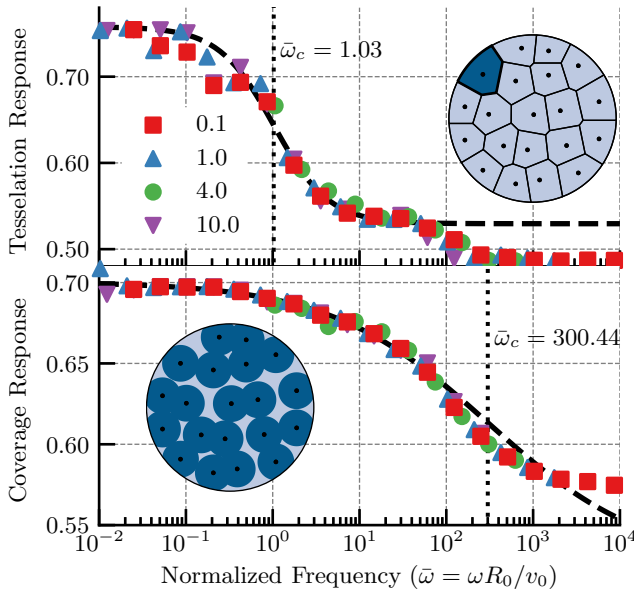


Fig. 5. Frequency response of a swarm of  $N = 20$  agents in dynamic area coverage according to its Tessellation performance  $P_T$  (top) and its Coverage performance  $P_C$  (bottom). The different markers correspond to calculations with different agent speeds  $v_0$ . The dashed line corresponds to the ideal performance of (11).

TABLE I  
PARAMETERS OF THE IDEAL PERFORMANCE (11) OBTAINED BY FITTING THE THEORETICAL RESPONSE OF AN IDEAL HOMOGENEOUS SYSTEM, MEASURED BOTH AS  $P_T$  AND  $P_C$ .

	Tessellation ( $P_T$ )	Coverage ( $P_C$ )
$P_0$	0.758	0.700
$P_\infty$	0.530	0.526
$\bar{\omega}_c$	1.03	300.44
$\lambda$	1.37	0.48

The cutoff frequency for tessellation performance is  $\omega_c \simeq v_0 / R_0$ . This is revealing that the capacity of the system to maintain a uniform configuration goes down as the boundaries of the target area move too fast for a single agent to follow them. In contrast, the cutoff frequency for the coverage performance is two orders of magnitude larger,  $\omega_c \simeq 300 v_0 / R_0$ , thus showing that the collective maintains the capacity to cover an area well beyond the individual agents’ limitations, an expected and sought feature of swarming systems.

### B. Ideal Heterogeneous Swarm

Next, we consider the case where the agents are not identical, and a fraction  $\rho_F$  of agents move at speed  $v_F = 2v_0$  while the rest move at  $v_0$ . The performance of the system could in principle have a complicated dependency on  $\rho_F$ ,  $v_0$ , and  $v_F$ . However, we observe that as long as the two speeds differ in approximately less than one order of magnitude, the performance only depends on these parameters through the mean speed of the collective,

$$\langle v \rangle = (1 - \rho_F)v_0 + \rho_F v_F. \quad (12)$$

The results are identical to the homogeneous case if one makes the substitution  $v_0 \rightarrow \langle v \rangle$ , see Fig. 6. Therefore, a heterogeneous swarm with a fraction  $\rho_F$  of agents moving twice as fast as the rest will have a cutoff frequency of the form

$$\omega_c(\rho_F) = (1 + \rho_F)\omega_c(\rho_F = 0). \quad (13)$$

## V. EXPERIMENTAL RESULTS

We have performed a series of field tests of dynamic area coverage using  $N = 22$  buoys deployed in an uncontrolled environment with no supporting infrastructure (Bedok Reservoir in Singapore). For each test, the collective is tasked with covering the dynamic area defined by (2) with an  $\alpha(t)$  oscillating at a certain frequency  $\omega$ . Given the parameters of the test ( $R_0 = 25$  m and  $v_0 \simeq 0.5$  m/s), the system is expected to have a collective cutoff frequency of approximately  $\omega_c = 0.02$  s<sup>-1</sup>. This means that, in general, one expects the swarm of buoys to be able to respond to changes in coverage at a time scale of approximately 1 minute when covering areas of the order of 1000 m<sup>2</sup>. The evolution of the Coverage performance  $P_C$ , and Tessellation performance  $P_T$  for one of these experiments is presented in Fig. 7.

As the core of this study is about heterogeneous swarming, we have also carried out a series of tests to study the effect

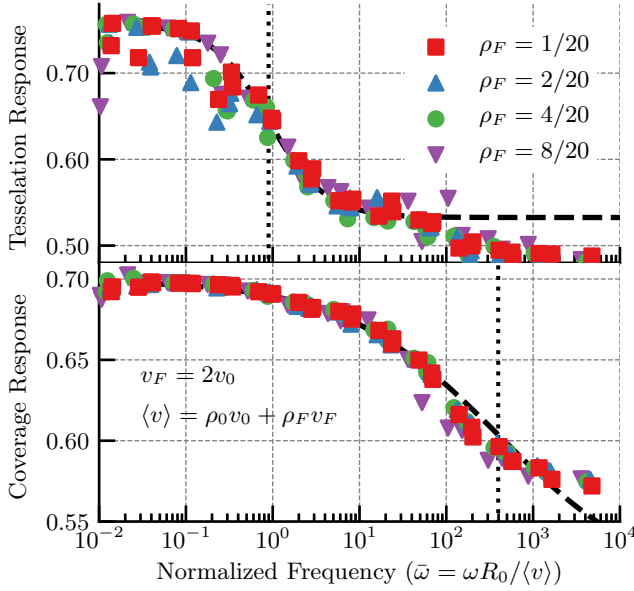


Fig. 6. Frequency response of a heterogeneous swarm of  $N = 20$  agents where a fraction  $\rho_F$  of them move twice as fast as the rest, measured by its Tessellation performance (top) and Coverage performance (bottom). The different markers correspond to calculations with different fractions of fast agents. Note that the frequency is normalized using the average speed, which depends on  $\rho_F$ .

of replacing a small portion ( $\rho_F = 4/22$ ) of the  $v_1$  buoys by the faster and improved model—design  $v_2$  presented in Sec. II. The theoretical prediction (see Fig. 6) using an idealized model is that this heterogeneous system would display a similar performance to the homogeneous case but with the frequencies shifted by  $\omega \rightarrow (1 + \rho_F)\omega = 1.18\omega$ . The experimental results for a total of 7 field tests are presented in Fig. 8. The overall performance of the homogeneous system, measured either by the tessellation or coverage metrics, is about 25% lower than the ideal case. This is a consequence of (i) the real dynamics and controllability of the buoys, (ii) the precision and accuracy of the GPS-based localization, and (iii) the finite communication rate between buoys as part of the distributed communication network. All these factors contribute to some extent, to the fact that the spatial distribution of the buoys is not as uniform as the cooperative control algorithm allows for.

Introducing heterogeneity in the real swarming system yields interesting results regarding its collective response (see Fig. 8). Instead of slightly improving both performance metrics as in the ideal case (see Sec. IV), what we observe is that a small proportion ( $\rho_F = 4/22 \simeq 18\%$ ) of faster buoys dramatically improves the coverage performance of the system while having a negligible effect on the tessellation performance.

As discussed before, the tessellation metric measures the performance of the system at the location where the deployment is the *least* uniform, and it is therefore primarily sensitive to the worst-performing section of the system. The coverage metric, in contrast, takes into account the deployment of all buoys and thus measures the system-level performance of

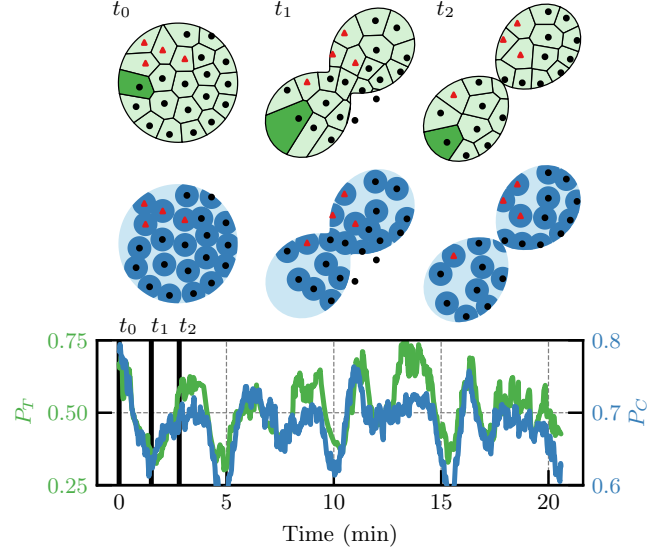


Fig. 7. Evolution of the two metrics for collective response  $P_T$  and  $P_C$  during a field experiment. The top panels show the distribution of the 18  $v_1$  buoys (black dots) and 4  $v_2$  ones (red triangles), along with the post-processed tessellation (top) and coverage (bottom). The frequency of the target area oscillations is  $\omega = 0.02 \text{ s}^{-1}$ , close to the theoretically predicted cutoff frequency of the collective.

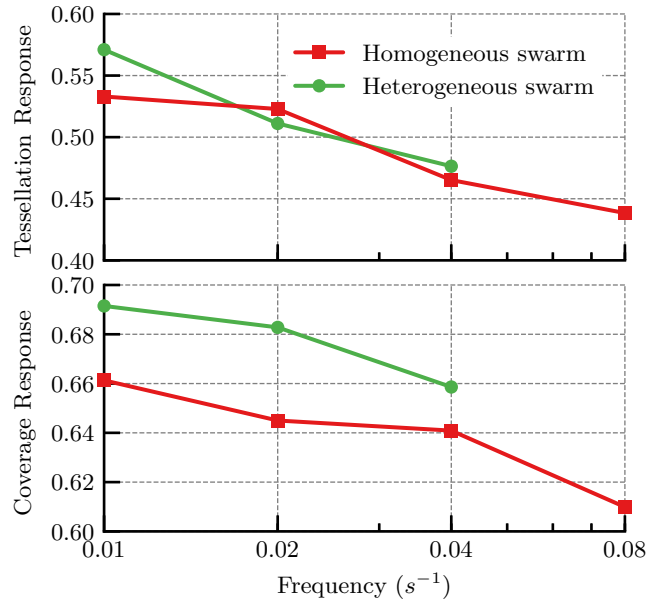


Fig. 8. Experimental frequency response of a swarm of buoys tasked with dynamic area coverage. The homogeneous system is composed of 22  $v_1$  buoys while the heterogeneous case has 18  $v_1$  and 4  $v_2$ .

this swarming system. These experimental observations reveal how the heterogeneity affects the operations of the system. Since the agents form a regular lattice in the target area and have a relatively small mobility within that lattice, the faster buoys (v2) can only use their higher speed to improve the deployment in the vicinity of their location in the lattice. This improvement always translates into an improved average performance, and thus an improved coverage. However, if the worst-performing agent happens to be far from the v2 buoys—e.g. in the snapshots of Fig. 7, these cannot affect its performance, and thus the tessellation performance remains virtually the same as in the heterogeneous case.

## VI. DISCUSSION

The efficient collective operation of heterogeneous swarms has been identified as one of the key challenges in robotics [15]. In general, such a swarm can be composed of a large number of different classes of agents where some may be specialized in specific tasks such as sensing, communications, or (sensed) data processing. However, with complex systems yielding emergent behaviors, it is not obvious that such individual enhancements of a fraction of the agents automatically translate into an increased collective performance. In this work, we study the effect of increasing the motor capabilities of 18% of the agents on the responsiveness of the group when performing a dynamic area monitoring in real-world and unstructured water environments.

Experimentally, we observe that the timescale at which the system is able to respond is in good agreement with the theoretical prediction, confirming that this distributed smart sensor array of buoys is capable of responding to changing environments on the order of the minute, which is well beyond what is needed to track morphological changes in oil spills, algal blooms, or other surface contaminants.

We also present empirical evidence that the partial upgrade of the system improves the responsiveness of the system when using a cooperative control algorithm designed for homogeneous systems and that does not explicitly take into account the different motor capabilities of the heterogeneous set of agents. We measure the performance of the system with two metrics, the tessellation  $P_T$  and the coverage  $P_C$  performances. Since  $P_T$  only takes into account the agent with the largest area to cover, it is an individual measure of the “weakest link” in the system. As such, it is indicative of the robustness of the collective.  $P_C$ , on the other hand, measures an average collective performance that is less sensitive to any individual agent’s behavior. While the partial upgrade makes the system more capable of dynamically covering a target area on average ( $P_C$ ), it does not improve the coverage of the least-covered regions ( $P_T$ ).

In order to magnify the effect of the new and improved agents, the system would need to operate taking into account the specific properties of the different agents. For instance, a further improvement in the collective responsiveness of this heterogeneous swarm could be achieved by developing a new cooperative control strategy that positions the faster agents

in the most critical areas, or that implements an optimization procedure constrained by the motor capabilities of the different agents. Such a procedure, however, could prove difficult to maintain as it is not robust to hardware design changes: as more kinds of agents are added during the life-cycle of the collective, the control algorithm should grow in complexity to accommodate these changes.

## ACKNOWLEDGMENTS

This work was supported by Grants from the SUTD-MIT International Design Center (IDC) and the Singapore Ministry of Education (MOE-Tier 1 Grant #T1MOE1701). We are grateful for the assistance of B. Patel, H. Shekhar, S. Jain, and P. Rastogi in preparing and performing the field tests described in this work.

## REFERENCES

- [1] J. E. Manley, “Unmanned surface vehicles, 15 years of development,” in *OCEANS 2008*, pp. 1–4, IEEE, 2008.
- [2] P. M. Orton, W. R. McGillis, J. R. Moisan, J. R. Higinbotham, and C. Schirtzinger, “The Mobile Buoy: An Autonomous Surface Vehicle for Integrated Ocean-Atmosphere Studies,” *AGU Spring Meeting Abstracts*, May 2009.
- [3] B. Bayat, N. Crasta, A. Crespi, A. M. Pascoal, and A. Ijspeert, “Environmental monitoring using autonomous vehicles: a survey of recent searching techniques,” *Current Opinion in Biotechnology*, vol. 45, pp. 76–84, 2017.
- [4] L. Zicarelli, R. Dellor, R. Johnson, H. Schmitz, T. O’Reilly, and F. Chavez, “A novel method of obtaining near real-time observations of phytoplankton from a mobile autonomous platform,” in *OCEANS 2016 MTS/IEEE Monterey*, pp. 1–5, IEEE, 2016.
- [5] H. Ferreira, C. Almeida, A. Martins, J. Almeida, N. Dias, A. Dias, and E. Silva, “Autonomous bathymetry for risk assessment with roaz robotic surface vehicle,” in *OCEANS 2009-Europe*, pp. 1–6, IEEE, 2009.
- [6] R. Bouffanais, *Design and Control of Swarm Dynamics*. Heidelberg: Springer, 2016.
- [7] M. Chamanbaz, D. Mateo, B. M. Zoss, G. Tokić, E. Wilhelm, R. Bouffanais, and D. K. P. Yue, “Swarm-enabling technology for multi-robot systems,” *Front. Robot. AI*, vol. 4, p. Art. 12, 2017.
- [8] A. Matos, R. Almeida, and N. Cruz, “Man portable acoustic navigation buoys,” in *Proc. of OCEANS 2016 - Shanghai*, pp. 1–6, 2016.
- [9] Y. Nishida, J. Kojima, Y. Ito, K. Tamura, H. Sugimatsu, K. Kim, T. Sudo, and T. Ura, “Development of an autonomous buoy system for AUV,” in *Proc. of OCEANS 2015 - Genova*, pp. 1–6, 2015.
- [10] G. Pico, J. Miranda, K. Marentes, and S. Tosunoglu, “Multipurpose autonomous buoy,” in *Proc. of the 29th Florida Conference on Recent Advances in Robotics, Miami, Florida*, pp. 128–144, 2016.
- [11] J. Vesecky, K. Laws, S. Petersen, C. Bazeghi, and D. Wiberg, “Prototype autonomous mini-buoy for use in a wireless networked, ocean surface sensor array,” in *Proc. of IEEE International Geoscience and Remote Sensing Symposium*, pp. 4987–4990, 2007.
- [12] B. M. Zoss, D. Mateo, Y. K. Kuan, G. Tokić, M. Chamanbaz, L. Goh, F. Vallegria, R. Bouffanais, and D. K. P. Yue, “Distributed system of autonomous buoys for scalable deployment and monitoring of large waterbodies,” *Autonomous Robots*, Feb 2018.
- [13] D. Mateo, Y. K. Kuan, and R. Bouffanais, “Effect of correlations in swarms on collective response,” *Sci. Rep.*, vol. 7, p. 10388, 2017.
- [14] Y. Shang and R. Bouffanais, “Consensus reaching in swarms ruled by a hybrid metric-topological distance,” *Eur. Phys. J. B*, vol. 87, p. 294, 2014.
- [15] G.-Z. Yang, J. Bellingham, P. E. Dupont, P. Fischer, L. Floridi, R. Full, N. Jacobstein, V. Kumar, M. McNutt, R. Merrifield, B. J. Nelson, B. Scassellati, M. Taddeo, R. Taylor, M. Veloso, Z. L. Wang, and R. Wood, “The grand challenges of science robotics,” *Science Robotics*, vol. 3, no. 14, 2018.